RECRYSTALLIZATION BEHAVIORS OF ALLOY IC10 AT ELEVATED TEMPERATURE

Zhang Hongjian, Wen Weidong, Cui Haitao

(College of Energy and Power Engineering, NUAA, 29 Yudao Street, Nanjing, 210016, P. R. China)

Abstract: To investigate recrystallization behaviors of the alloy IC10, tensile experiments are conducted over a wide range of strain rates (10^{-4}—10^{-2} s^{-1}) at 900 ℃ by using a material testing system (MTS809). Experimental results show that: (1) The flow stress is sensitive to the strain rate while the stress-strain curve at various strain rates exhibit the similar features; (2) The flow stress, the critical stress and the critical strain increase with strain rates. And the mechanisms of these properties are studied based on the examinations of transmission electron microscopy (TEM) and scanning electron microscopy (SEM). In order to study the flow features of IC10, a new phenomenological constitutive model is developed. The effectiveness of the model is verified by extensive experiments on IC10.

Key words: constitutive models; recrystallization; alloy IC10

CLC number: TB124; TB35 **Document code**: A **Article ID**: 1005-1120(2011)01-0081-06

INTRODUCTION

In recent years, ordered Ni_3Al based intermetallic compounds have been intensively studied as the potential high temperature structural materials in the aerospace applications, e. g., turbine engine components. Such materials have the features of high specific modules, high yield strength, fairly good ductility from room temperature to elevated temperature, high incipient melting temperature, excellent oxidation resistance, and high creep resistance over a wide range of temperatures. Alloy IC10 is a newly developed Ni_3Al based superalloy, which can be used as advanced aero-engine van materials at service temperature that is 1 373 K[1].

Extensive studies are made for the applications of alloy IC10. And various constitutive models are developed to describe the strain hardening behaviors at different temperatures and strain rates[2-6]. But the studies about the recrystallization behaviors of alloy IC10 at elevated temperatures are still rare.

The evolution of the microstructure under high temperatures involves strain hardening, dynamic recovery, recrystallization, and grain growth, all of which are highly related to temperature and strain rate. In particular, recrystallization leads to the local elimination of a large number of dislocations and is generally associated with a decrease in the average grain size. Although state-variable based constitutive equations for materials undergoing hot work are successful in describing strain hardening and dynamic recovery, the limited work are performed in addressing dynamic recrystallization within a continuum framework.

In this paper, the recrystallization and the fracture behaviors of IC10 are investigated based on experiments, and a new phenomenological constitutive model is developed to describe the recrystallization behaviors. The effectiveness of the model is also verified by the extensive experiments on IC10.

Foundation item: Supported by the Aviation Science Foundation of China (08B52002).

Received date: 2010-10-18; **revision received date**: 2011-01-10

E-mail: zhanghongjian@nuaa.edu.cn

1 EXPERIMENTAL PROCEDURES AND RESULTS

1.1 Experimental procedures

Ni_3Al based alloy IC10, supplied by the AVIC1 Beijing Institute of Aeronautical Materials, is a directional solidification material in [001] orientation with its nominal composition (in weight): 0.07%—0.12%C, 11.5%—12.5%Co, 6.5%—7.5%Cr, 5.6%—6.2%Al, 4.8%—5.2%W, 1.0%—2.0%Mo, 6.5%—7.5%Ta, 1.3%—1.7%Hf, 0.01%—0.02% B, and Bal. Ni. The alloy is prepared by vacuum induction furnace and followed by casting to ingots. The column tensile specimens with dimension of Φ10 mm×50 mm are machined from the bars.

To investigate recrystallizational behaviors of IC10, tensile experiments are carried out at four different strain rates (10^{-2}, 10^{-3}, 5×10^{-4}, and 10^{-4} s^{-1}) under the temperature of 900 ℃, which is attained with a high-intensity quartz lamp in a radiant-heating furnace (MTS653 furnace). All tests are conducted with MTS809 system, a computer-controlled, servo-hydraulic tensile torsion machine. All the specimens are strained to fracture and then cooled in the air to room temperature. The experimental data are gathered with the signal automatism gather system of MTS809.

To characterize fracture behaviors of IC10, the deformed specimens are observed by scanning electron microscopy (SEM) examinations on a JSM-5600LV SEM. The transmission electron microscopy (TEM) examinations are operated to describe the deformation mechanisms. For TEM examinations, slices parallel and vertical to the tensile axis are cut from specimens by spark erosion. The foils are prepared by using twin-jet electropolishing and examined on a JEM-2010 analytical transmission electron microscope.

1.2 Experimental results

The stress-strain(σ-ε) curves recorded at different strain rates (10^{-2},10^{-3},5×10^{-4}, and 10^{-4} s^{-1}) under 900 ℃ are shown in Fig. 1. As shown in Fig. 1, the flow stress is sensitive to the strain rate. But the stress-strain curve at every stain rate exhibits similar features: firstly the flow stress positively increases with the strain before the critical strain, and then the softening happens after the critical strain, which is the typical dynamic recrystallization curve. A close comparison among these curves at different strain rates reveals that the flow stress, the critical stress and the critical strain increase with strain rates.

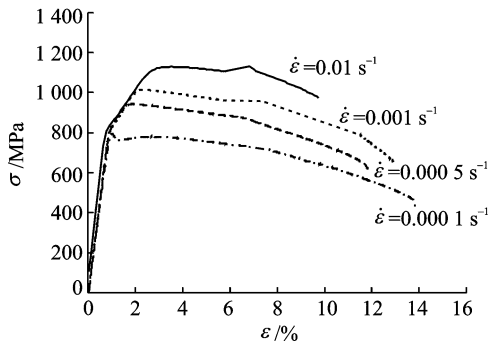

Fig. 1 σ-ε curves at 900 ℃

Fig. 2 shows one of the typical bright-field images of dislocation structures in foils from specimens deformed to fracture at 900 ℃. As shown in Fig. 2, the dislocations have a tendency to form either edge or screw segments on the cube plane so that almost regular square nets of dislocations can be observed. A great number of dislocation nets lead to the formation of the slipbands at phase boundaries. During the formation process, a lot of dislocations are annihilated, thus leading to the decrease of dislocation density and the softening effect of material. It is known that the dislocation greatly multiply in the process of deformation. And the multiplication can lead to the hardening effect of material. At the beginning of

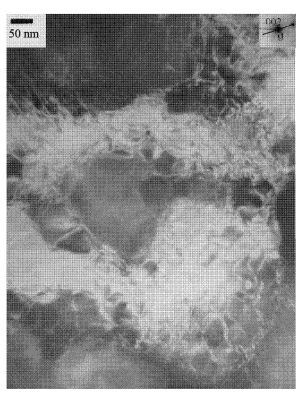

Fig. 2 Bright-field image

deformation, the multiplication rate is greater than the annihilation rate, and the hardening effect dominates. When the dislocation density achieves a critical value, the multiplication rate is equal to the annihilation rate, and the flow stress gets saturation. After that, the softening effect can colltrol the deformation if the multiplication rate is less than the annihilation rate. That is the mechanism of recrystallization behavior of metals.

Fig. 3 is one of the typical SEM images of fracture surface of alloy IC10 at 900 ℃, and shows that the fracture is the dimple fracture character mixed with a few of intergranular.

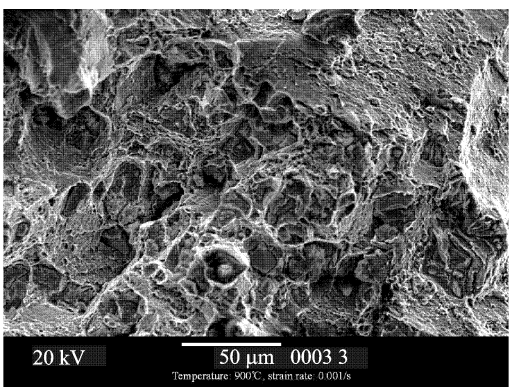

Fig. 3 SEM image

2 DEVELOPMENT OF CONSTITUTIVE EQUATION

A new constitutive model is proposed for describing the recrystallization behaviors as following formulations

$$\sigma = \sigma_c - K(\Delta\varepsilon)^n = \begin{cases} \sigma_c - K_h(\varepsilon_c - \varepsilon)^{n_h} & \varepsilon \leqslant \varepsilon_c \\ \sigma_c - K_s(\varepsilon - \varepsilon_c)^{n_s} & \varepsilon > \varepsilon_c \end{cases} \tag{1}$$

where σ is the stress, $K(K_h, K_s)$ and $n(n_h, n_s)$ are the parameters. The subscripts (h and s) refer to strain hardening part before the critical strain ε_c, and softening part after the critical strain ε_c, respectively. σ_c is the critical stress at the strain of ε_c. $\Delta\varepsilon$ is equal to $|\varepsilon_c - \varepsilon|$.

As seen from Eq. (1), the formulation $\sigma = \sigma_c - K_h(\varepsilon_c - \varepsilon)^{n_h}$ is used to describe the strain hardening part, and the equation $\sigma = \sigma_c - K_s(\varepsilon - \varepsilon_c)^{n_s}$ is the softening part.

Normally, the feature of the stress-strain curve is determined by the parameters (K and n), which are assumed to be constants at a decided experiment condition and vary with the mechanical properties, such as yield stress $\sigma_{0.2}$, critical stress/strain (σ_c/ε_c), fracture stress σ_f, and elongation ε_f. The variation rules are discussed in the following section.

When ε is equal to ε_1 (ε_1 is a random point in the curve), Eq. (1) follows that

$$\sigma_1 = \sigma_c - K(\Delta\varepsilon_1)^n \tag{2}$$

From Eq. (2), we obtain

$$K = \frac{\sigma_c - \sigma_1}{(\Delta\varepsilon_1)^n} \tag{3}$$

When ε is equal to $\varepsilon_{0.2}$, the stress is the yield stress $\sigma_{0.2}$, we obtain

$$\sigma_{0.2} = \sigma_c - K_h(\Delta\varepsilon_{0.2})^{n_h} = \sigma_c - K_h(\varepsilon_c - \varepsilon_{0.2})^{n_h} \tag{4}$$

When ε is equal to ε_f, the stress is the broken strength σ_f. Eq. (1) follows that

$$\sigma_f = \sigma_c - K_s(\Delta\varepsilon_f)^{n_s} = \sigma_c - K_s(\varepsilon_f - \varepsilon_c)^{n_s} \tag{5}$$

When ε_1 is less than ε_c, and let Eq. (4) divide Eq. (2), we obtain

$$n_h = \frac{\ln\left(\dfrac{\sigma_c - \sigma_{0.2}}{\sigma_c - \sigma_1}\right)}{\ln\left(\dfrac{\Delta\varepsilon_{0.2}}{\Delta\varepsilon_1}\right)} \tag{6}$$

When ε_1 is greater than ε_c, and let Eq. (5) divide Eq. (2), we obtain

$$n_s = \frac{\ln\left(\dfrac{\sigma_c - \sigma_f}{\sigma_c - \sigma_1}\right)}{\ln\left(\dfrac{\Delta\varepsilon_f}{\Delta\varepsilon_1}\right)} \tag{7}$$

When $\Delta\varepsilon = \Delta\varepsilon_1 = 1\%$, in order to describe the hardening part, the following equations are obtained from Eqs. (3,6).

$$K_h = \sigma_c - \sigma_1 \propto \frac{\sigma_c - \sigma_{0.2}}{\Delta\varepsilon_{0.2}} \tag{8}$$

$$n_h = \frac{\ln\left(\dfrac{\sigma_c - \sigma_{0.2}}{\sigma_c - \sigma_1}\right)}{\ln(\Delta\varepsilon_{0.2})} \propto \frac{\ln(\sigma_c - \sigma_{0.2})}{\ln(\Delta\varepsilon_{0.2})} \tag{9}$$

As $\Delta\varepsilon = \Delta\varepsilon_1 = 1\%$, when describing the softening part, the following equations are obtained from Eqs. (3,7).

$$K_s = \sigma_c - \sigma_f \propto \frac{\sigma_c - \sigma_f}{\Delta\varepsilon_f} \tag{10}$$

$$n_s = \frac{\ln\left(\dfrac{\sigma_c - \sigma_f}{\sigma_c - \sigma_1}\right)}{\ln(\Delta\varepsilon_f)} \propto \frac{\ln(\sigma_c - \sigma_f)}{\ln(\Delta\varepsilon_f)} \tag{11}$$

As seen in Eqs. (8-11), the variation of the parameters K and n at different conditions can be described by the mechanical properties, such as critical stress σ_c, yield stress $\sigma_{0.2}$, fracture strength σ_f, $\Delta\varepsilon_{0.2}$ and $\Delta\varepsilon_f$. The relationships between the parameters (K and n) and the mechanical properties follow that

$$K_1 : K_2 = \begin{cases} K_{h1} : K_{h2} \approx \left(\dfrac{\sigma_c - \sigma_{0.2}}{\Delta\varepsilon_{0.2}}\right)_1 : \left(\dfrac{\sigma_c - \sigma_{0.2}}{\Delta\varepsilon_{0.2}}\right)_2 \\ \qquad \varepsilon \leqslant \varepsilon_c \\ K_{s1} : K_{s2} \approx \left(\dfrac{\sigma_c - \sigma_f}{\Delta\varepsilon_f}\right)_1 : \left(\dfrac{\sigma_c - \sigma_f}{\Delta\varepsilon_f}\right)_2 \\ \qquad \varepsilon > \varepsilon_c \end{cases} \tag{12}$$

$$n_1 : n_2 = \begin{cases} n_{h1} : n_{h2} \approx \left(\dfrac{\ln(\sigma_c - \sigma_{0.2})}{\ln(\Delta\varepsilon_{0.2})}\right)_1 : \\ \quad \left(\dfrac{\ln(\sigma_c - \sigma_{0.2})}{\ln(\Delta\varepsilon_{0.2})}\right)_2 & \varepsilon \leqslant \varepsilon_c \\ n_{s1} : n_{s2} \approx \left(\dfrac{\ln(\sigma_c - \sigma_f)}{\ln(\Delta\varepsilon_f)}\right)_1 : \\ \quad \left(\dfrac{\ln(\sigma_c - \sigma_f)}{\ln(\Delta\varepsilon_f)}\right)_2 & \varepsilon > \varepsilon_c \end{cases} \tag{13}$$

The subscripts (1 and 2) in the two equations refer to the different experiment conditions.

Then, the constitutive equation can be obtained

$$\sigma = \begin{cases} \sigma_c - K_{hr} \dfrac{\left(\dfrac{\sigma_c - \sigma_{0.2}}{\Delta\varepsilon_{0.2}}\right)}{\left(\dfrac{\sigma_c - \sigma_{0.2}}{\Delta\varepsilon_{0.2}}\right)_r} \cdot \\ (\varepsilon_c - \varepsilon)^{n_{hr} * \left\{\frac{\left(\frac{\ln(\sigma_c - \sigma_{0.2})}{\ln(\Delta\varepsilon_{0.2})}\right)}{\left(\frac{\ln(\sigma_c - \sigma_{0.2})}{\ln(\Delta\varepsilon_{0.2})}\right)_r}\right\}} & \varepsilon \leqslant \varepsilon_c \\ \sigma_c - K_{sr} \dfrac{\left(\dfrac{\sigma_c - \sigma_f}{\Delta\varepsilon_f}\right)}{\left(\dfrac{\sigma_c - \sigma_f}{\Delta\varepsilon_f}\right)_r} \cdot \\ (\varepsilon - \varepsilon_c)^{n_{sr} * \left\{\frac{\left(\frac{\ln(\sigma_c - \sigma_f)}{\ln(\Delta\varepsilon_f)}\right)}{\left(\frac{\ln(\sigma_c - \sigma_f)}{\ln(\Delta\varepsilon_f)}\right)_r}\right\}} & \varepsilon > \varepsilon_c \end{cases} \tag{14}$$

The subscript letter "r" in the equation refers to the reference conditions.

3 APPLICATION, COMPARISONS AND DISCUSSION

In this section, the effectiveness of the newly developed model is verified by the extensive experiments on IC10.

The reference stress-strain curve is the one measured at the condition of 900 ℃ with strain rate $\dot{\varepsilon} = 10^{-2}\ \mathrm{s}^{-1}$. The parameters ($K$ and n) are obtained by fitting the reference curve using Eq. (1). The fitted parameters are listed in Table 1.

Table 1 Values of parameters K and n

Parameter	K_{hr}	n_{hr}	K_{sr}	n_{sr}
Value	38.586 59	2.098 56	1.262 25	2.646 89

Fig. 4 shows the comparison of the experimental and the fitted data, and illustrates that the model fits in the experimental data well.

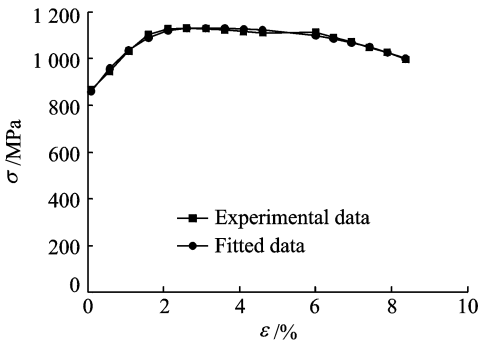

Fig. 4 Comparison of fitted and experimental data at 900 ℃ with $\dot{\varepsilon} = 10^{-2}\ \mathrm{s}^{-1}$

Then, the constitutive equations of IC10 follow that

$$\sigma = \begin{cases} \sigma_c - 38.586\ 59 \dfrac{\left(\dfrac{\sigma_c - \sigma_{0.2}}{\Delta\varepsilon_{0.2}}\right)}{105.752\ 7} \cdot \\ (\varepsilon_c - \varepsilon)^{2.098\ 56 * \frac{\left(\frac{\ln((\sigma_c - \sigma_{0.2}))}{\ln(\Delta\varepsilon_{0.2})}\right)}{5.855\ 75}} & \varepsilon \leqslant \varepsilon_c \\ \sigma_c - 1.262\ 25 \dfrac{\left(\dfrac{\sigma_c - \sigma_f}{\Delta\varepsilon_f}\right)}{25.605\ 23} \cdot \\ (\varepsilon - \varepsilon_c)^{2.646\ 89 * \frac{\left(\frac{\ln(\sigma_c - \sigma_f)}{\ln(\Delta\varepsilon_f)}\right)}{2.788\ 04}} & \varepsilon > \varepsilon_c \end{cases} \tag{15}$$

The values of the mechanical properties measured with the tensile experiments are listed in Table 2.

Table 2 Values of mechanical properties (measured by tensile experiments)

$\dot{\varepsilon}/\mathrm{s}^{-1}$	$\sigma_{0.2}$/MPa	σ_c/MPa	ε_c/%	σ_f/MPa	ε_f/%
10^{-2} (reference state)	853.150	1 129.320	2.611	972.296	9.755
10^{-3}	840.650	1 013.000	1.378	643.263	12.945
5×10^{-4}	855.232	943.247	0.726	618.160	11.815
10^{-4}	785.270	785.270	0.000	425.176	13.821

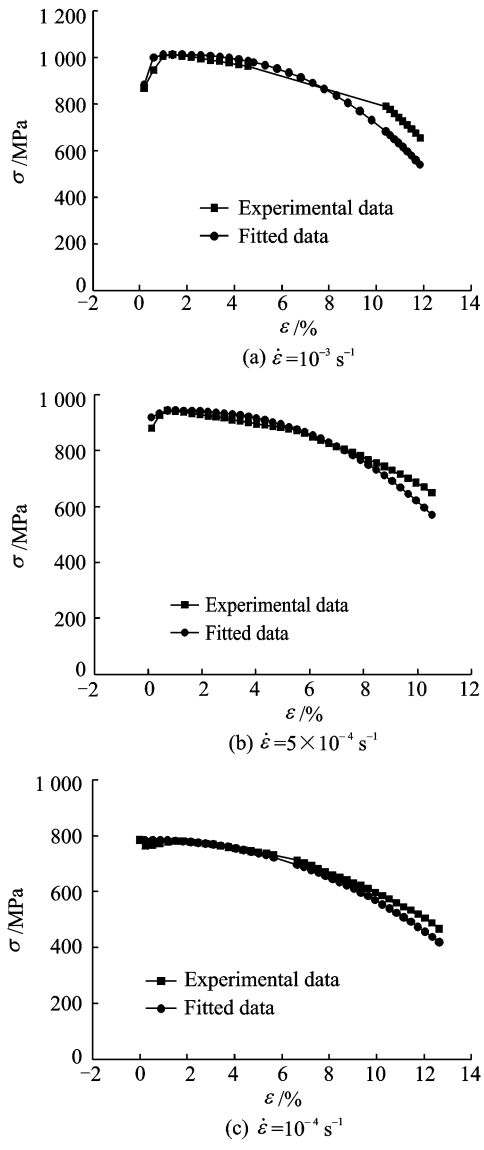

Fig. 5 Comparison of predicted and experimental data at 900 ℃

The constitutive equation predicting a new curve can be obtained on the basis of the mechanical properties (listed in Table 2) and Eq. (15).

Fig. 5 shows the comparisons between the data predicted by the new model and the experiment. The predicted data fit well with the experiment, which indicates that the new model is feasible to describe recrystallization behaviors of alloy IC10.

4 CONCLUSIONS

(1) Based on the tensile experiments, the flow behaviors of IC10 at 900 ℃ are studied. Experiments show that the dynamic recrystallizationis the domination phenomena and the flow stress is sensitive to the strain rate.

(2) Based on the TEM and SEM experiments, the deformation and the fracture mechanisms are studied. Experiments show: the mechanism of recrystallization behavior is that the dislocations have a tendency to form almost regular square nets at phase boundaries; and the fracture mechanism is the dimple fracture mixed with a few of intergranular.

(3) A new model is developed and used to describe the recrystallization behaviors of alloy IC10. The predicted data fit well with the experiments.

References:

[1] Zhao Xihong, Huang Zhaohui, Tan Yongning, et al. New Ni3Al-Based directionally-solidified superalloy IC10[J]. Journal of Aeronautical Materials, 2006, 26(3):20-24. (in Chinese)

[2] Zhang Hongjian, Wen Weidong, Cui Haitao, et al. Constitutive analysis of alloy IC10 at different temperatures[J]. Acta Aeronautica Et Astronautica Sinica, 2008, 29(2):499-504. (in Chinese)

[3] Zhang Hongjian, Wen Weidong, Cui Haitao. Behaviors of IC10 alloy over a wide range of strain rates and temperatures: experiments and modeling[J]. Materials Science & Engineering A, 2009, 504: 99-103.

[4] Zhang Hongjian, Wen Weidong, Cui Haitao, et al. A study on flow behaviors of alloy IC10 over a wide range of temperatures and strain rates[C]//2008 TMS Annual Meeting & Exhibition on Materials for High Temperature Applications: Next Generation Superalloys and Beyond. San Francisco, California, USA:[s. n.], 2009: 219-226.

[5] Zhang Hongjian, Wen Weidong, Cui Haitao, et al. Modification of Z-A model and the prediction of the constitutive model[J]. Journal of Aerospace Power, 2009, 24(6): 1311-1315. (in Chinese)

[6] Zhang Hongjian, Wen Weidong, Cui Haitao, et al. A modified Zerilli-Armstrong model for alloy IC10 over a wide range of temperatures and strain rates [J]. Materials Science & Engineering A, 2009,527: 328-333.

高温下IC10合金的动态再结晶特性研究

张宏建 温卫东 崔海涛
(南京航空航天大学能源与动力学院,南京,210016,中国)

摘要:为了研究IC10合金的动态再结晶特性,利用MTS809材料测试系统对其在900 ℃、不同应变率(10^{-4}~10^{-2} s^{-1})下进行了拉伸试验。试验结果表明:(1) 不同应变率下的应力-应变曲线具有类似的特征,并且IC10合金的流变应力对应变率敏感;(2) 流变应力、临界应力和临界应变随着应变率的增加而增大。基于TEM和SEM试验IC10合金的力学特性机理。为了描述IC10合金的动态再结晶行为,本文提出了一个新的宏观唯象本构模型。该模型的预测与试验结果比较验证了其有效性。

关键词:本构模型; 动态再结晶; IC10合金
中图分类号:TB124; TB35

(Executive editor: Zhang Huangqun)

基金项目:国家航空科技创新基金 (08B52002) 资助项目。